# Turning motion of multi-connection cross-flow vertical axis offshore wind turbines tension-moored at a single point

Saika Iwamatsu[1*], Kazuma Kusanagi[2†], Sharath Srinivasamurthy[3†], Kazuhiro Iijima[4†], Tomoki Ikoma[5†] and Yasunori Nihe[6†]

[1*]Department of Aerospace and Marine System Engineering, Osaka Prefecture University, 1-1 Gakuen-cho, Sakai-shi, 5998531, Osaka, Japan.

[2]Mechanical & Electrical Division Electrical Instrumentation Group Engineering Department, KOBELCO E&M Co., Ltd., 4-5-22 Iwayakita-machi, Kobe-shi, 6570846, Hyogo, Japan.

[3]Institute of Ocean Energy, Saga University (IOES), 1 Honjo-machi, Saga-shi, 8408502, Saga, Japan.

[4]Department of Naval Architecture, Osaka University, 1-1 Yamada, Suita, 5650871, Osaka, Japan.

[5]Department of Oceanic Architecture and Engineering, Nihon University, 7-24-1 Narashinodai, Funabashi-shi, 2748501, Chiba, Japan.

[6]Department of Aerospace and Marine System Engineering, Osaka Metropolitan University, 1-1 Gakuen-cho, Sakai-shi, 5998531, Osaka, Japan.

*Corresponding author(s). E-mail(s): de102001@st.osakafu-u.ac.jp;
Contributing authors: k.kusanagi1101@gmail.com; sharath@cc.saga-u.ac.jp; iijima@naoe.eng.osaka-u.ac.jp; ikoma.tomoki@nihon-u.ac.jp; nihei@omu.ac.jp;
†These authors contributed equally to this work.

**Abstract**

This study proposes a Multi-connection cross-flow vertical axis wind turbine (VAWT), an innovative device to supply electric power in aquaculture farms. The device is a newtype floating offshore wind turbine (FOWT) consisting of two independent wind turbine floats and a mooring float set in a straight line. A Single-Point-Mooring (SPM) system with tension is utilized at the mooring float, which allows the wind turbine floats to turn around the moored point. However, there are various challenges to this new concept for its practical application mainly related to turning motion about the moored point. Therefore, the focus of this study is to understand the turning mechanism of the proposed FOWT through dedicated water tank experiments and numerical simulations. As a concept demonstration, two cross-flow wind turbines, were mounted on the wind turbine floats and turning motion characteristics about the moored point is observed. A prototype model was built with a model scale of 1/36 using Froude scaling assuming rough weather conditions at the aquaculture farm. Wind speed of 35 m/s, wave height of 0.75 m, and wave period of 5 to 7.5 s, are the assumed environmental conditions in the actual model. Free yawing tests were conducted in only-wind, only wave and combined wind-wave conditions. Further, a numerical simulation considering the wind loads acting on the turbines is developed. It is found that the wind turbine floats turn to a position where the wind loads acting on the left and right sides of the moored point are balanced. The numerical simulation reproduced the turning motion within an error of 10

# 1 Introduction

Marine environment is rapidly changing and phenomenon such as red tide and anoxic water mass, are occurring in aquaculture farms. This causes damage to fish and shellfish production, and has negative impact to aquaculture farms in Japan. The deterioration of water quality in aquaculture farms is caused by the concentration of nutrients and the lack of oxygen in the lower water layers. A common solution to red tide is the application of clay, which is effective in controlling red tide. This method has been proven by Maeda et al (2009) to destroy red tide plankton in a short period of time with no impact on the ecosystem, and is used worldwide as a red tide countermeasure. As a solution to the anoxic water masses, aeration devices that supply oxygen to seawater by exposing it to air and seawater circulation pumps that mix the upper and lower layers of seawater can be utilized. However, unlike solutions for red tides, many of the solutions for anoxic water masses require electric power, which is difficult to secure at sea. Therefore, it is necessary to solve the problem of securing electric power in aquaculture farms.

There are three types of offshore power supply: photovoltaic, tidal current and wind power. Photovoltaic power generation has already been introduced as above water photovoltaic power generation, and Thi et al (2021) proposed

its use and future potential in aquaculture farms. On the other hand, there are concerns about the deterioration of water quality due to the reduction of sunlight hours in the water and the damage to the solar panels caused by drifting debris. In Japan, Ueno et al (2018) conducted a demonstration study using a 100kW-class ocean current generator, and in the United States, several projects focusing on tidal current generation, such as Verdant Power LLC. (2019), are underway. However, water bodies where water quality degradation is an issue are not expected to generate enough current to generate electricity, due to limited or no water flow. Offshore wind power generation is one of the fields that have been rapidly being researched in recent years, and is attracting attention around the world.

Offshore wind turbines can be classified as bottom-fixed and floating types. In this study, the floating type will be used because it is easier to move after installation. Furthermore, there are three types of floating systems: pontoons, semi-submersibles, and spars. The pontoon type, also known as the barge type, has the shape of an ark. It maintains the stability of the floating body by increasing the waterline area, and can be installed in shallow waters with shallow draft. In this study, a tub type was chosen because it is simple to fabricate and can be installed in shallow water. Kikuchi et al (2017) found that the pontoon type tends to shorten the natural period in the heave and pitch directions compared to other types of floating structures but it resonates with waves, resulting in larger oscillations. However, the pontoon type can be applied to the aquaculture farm since it is assumed to be in a relatively calm sea area.

Another important aspect of floating structures is the mooring system to station them. Floating structures are usually installed on the seabed by multi-point catenary mooring, single point mooring, or tension mooring with different spring rates. Many floating wind turbines, such as the 2MW FOWT "Fukushima Mirai," combine multiple moorings with catenary mooring, a type of loose mooring, for stability and safety. "Fukushima Mirai" consists of three mooring points, and six catenary mooring lines spread every 120 degrees (Yamaguchi and Imakita (2018)). The water area assumed in this study is an aquaculture farm, and the multi-point mooring system and catenary mooring, which require a vast area, are not suitable. Alkan (2017) argue that TLPs have many advantages over catenary mooring, such as less turbulence. Furthermore, Iijima et al (2015) and Srinivasamurthy et al (2021) applied single-point mooring, which is usually used for FPSO, to a floating wind turbine and showed its usefulness.

In the view of the above discussions, we propose a multi-connection VAWTs (Vertical Axis Offshore Wind Turbine) as an effective means of preventing the deterioration of the aquaculture fishery environment. Multi-connection VAWTs is a new type of FOWT initially conceptualized by Kusanagi et al (2018), which consists of a wind turbine float and a moored float with two VAWTs installed in a straight line. A single point mooring system with four tension moorings is adopted to station it. The new concept proposed in this

study can be equipped with two vertical axis wind turbines in a single mooring unit. The Multi-connection VAWTs is a groundbreaking idea, since the existing technology generally uses the concept of one wind turbine per mooring. In addition, in anticipation of the larger size of this new FOWT, similar experiments (Iwamatsu et al (2021)) were conducted using two different semi-submersible floats hosting Darius-type wind turbines, and it demonstrated the usefulness of this new concept for Darius-type wind turbines.

Furthermore, one of the features of this concept is the use of vertical axis type wind turbines. Most of the existing floating wind turbines and onshore wind turbines are horizontal axis wind turbines. However, horizontal axis wind turbines are difficult to operate at sea because of the yaw control mechanism, which requires maintenance at a faster rate and is located at the tower top. In addition, the high location of the control mechanism increases the overall center of gravity, which is fatal for floating turbines. In contrast to horizontal axis wind turbines, vertical axis wind turbines are non-directional, which eliminates the need for a control mechanism and reduces the center of gravity of the floating structure. The concept of Multi-connection VAWTs combines a single-point mooring with vertical axis wind turbines, which enables multiple wind turbines to face the wind direction.

The Multi-connection VAWTs is a new type of floating wind turbine. The power generation efficiency of two vertical-axis wind turbines in a row has been studied by Giorgetti et al (2015), but it has not been clarified what kind of turning motion it performs when two VAWTs are utilized as offshore wind turbines. There are still many problems and unknown mechanisms to be addressed for its practical application. In this study, water tank experiments and numerical simulations are carried out. From the experiments, we will confirm whether the Multi-connection VAWTs actually follows the wind or not, and clarify the mechanism of wind-following of the floating body. In this paper, a prototype model with two VAWTs is used as a demonstration, and the concept development and operating principle of Multi-connection VAWTs are clarified by experimental results and numerical simulations.

## 2 Concept

Figure 1 shows the conceptual design of the proposed system. The feasibility of the concept is tested using twin-connected VAWTs. The test model consists of two types of floating bodies: wind turbine floats and mooring float. The wind turbine floats are equipped with two cross-flow type vertical axis wind turbines, one of which rotates clockwise and the other counterclockwise. The mooring float is stationed using a single point mooring system and connected to the center of the wind turbine floats. Therefore, the wind turbine floaters can rotate around the moored buoy.

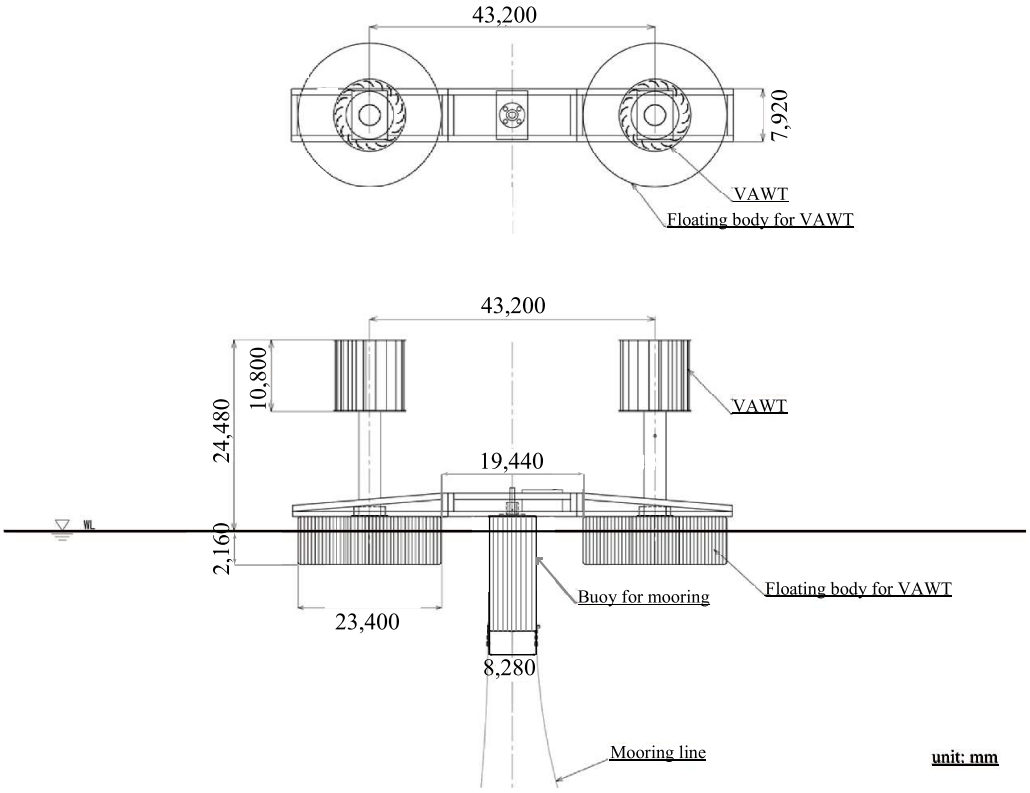


**Fig. 1** Concept design of Multi-connection VAWTs. (full scale)

Cross-flow wind turbines are vertical-axis wind turbines of the same drag type as Savonius wind turbines. As shown in Figure 2, drag-type wind turbines have inferior power generation performance compared to lift-type wind turbines. However, they are often installed as small wind turbines in residential areas because of their low RPM and higher safety. Nakata (2014) conducted study on performance of cross-flow wind turbines that can be installed on structures such as fences and buildings. In this study, too, a small cross-flow wind turbine was employed because the study envisions an aquaculture farm where fishing personnel would be working nearby.

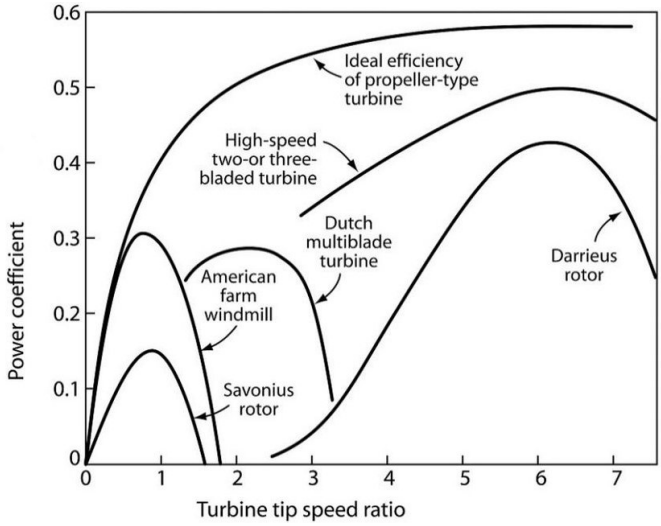


**Fig. 2** Performance curves for wind turbines. (Frank (1980))

When multiple wind turbines are installed, it is possible that they line up in the direction of the wind as elucidated in Figure 3 (a). When they overlap with respect to the wind direction, the wind turbine on the leeward side cannot receive enough wind due to wake effects. It has been confirmed by experiments that the rotational speed of the vertical axis wind turbine on the leeward side decreases by about 40-50% (Philip (2012)) compared to that on the upwind side and it depends on the distance between the wind turbines. However, in the proposed concept, the model itself can turn and receive maximum wind at all times (Figure 3(b)). Therefore, it is expected to generate stable power at various offshore sites using the proposed concept.

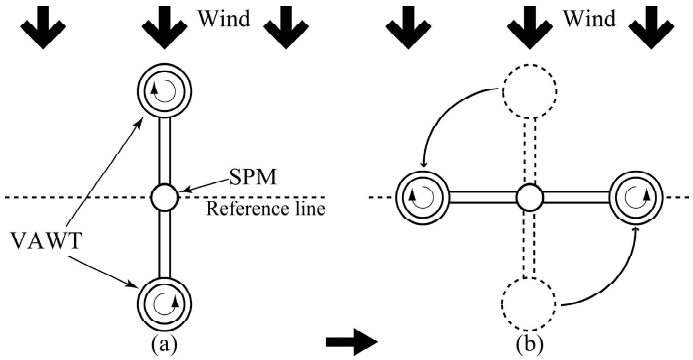


**Fig. 3** Turning motion of Multi-connection VAWTs.

# 3 Model design

## 3.1 Vertical axis wind turbine

A cross-flow type wind turbine, which is one of the vertical axis type wind turbines and has a track record of commercialization as a small wind turbine is adopted. The rotor part is made of aluminum, and the support part is made

of PVC pipe (Figure 4). The rotor consists of 18 blades and cross-sectional shape of each blade is a thin arc wing. This vertical axis type wind turbine is attached to the left and right sides of the wind turbine floater, one rotating clockwise and the other counterclockwise.

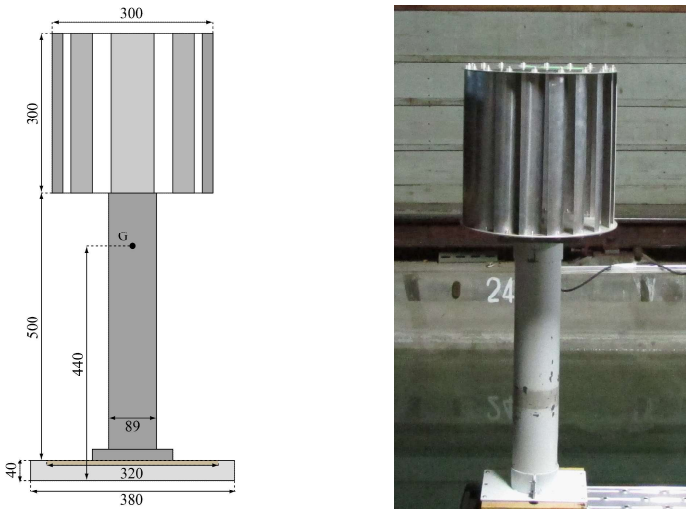


(a) Front view (b) Experimental model

**Fig. 4** Cross-flow type wind turbine from side

## 3.2 Wind turbine floaters

Wind floaters to host the turbines is shown in the Figure 5. The two floaters are connected at the top using a single frame structure, such that twin turbines can be connected to the mooring buoy. The wind turbine floaters are made of aluminum and frame is made of aluminum. Figure 6 shows the wind turbine floaters hosting the cross-flow type turbine built for the experiment. Table 1 tabulates the principal particulars of the experimental model.

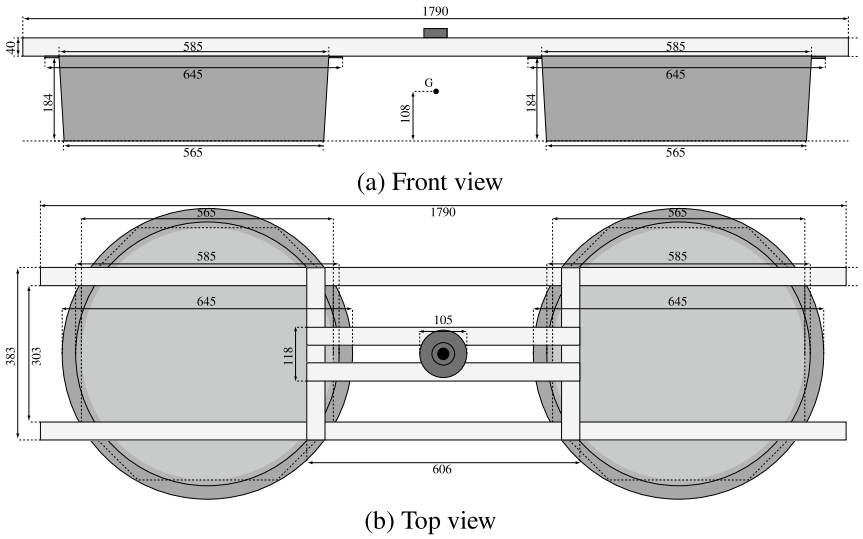


**Fig. 5** Wind turbine floaters

**Fig. 6** Experimental model with wind turbines

**Table 1** Principal particulars of the experimental and actual model wind float body (equipped with a wind turbine, overall system)

| Item | Unit | Scale Model | Actual Model |
|---|---|---|---|
| Mass | ton | 0.03 | 1430.47 |
| Draft | m | 0.06 | 2.16 |
| KB | m | 0.03 | 1.08 |
| KG | m | 0.30 | 10.80 |
| BM | m | 0.32 | 11.52 |
| GM | m | 0.05 | 1.80 |

## 3.3 Mooring buoy floater

The mooring buoy floater has a cylindrical shape made of PVC pipe and both ends of the pipe are covered with acrylic disks. The upper part of the mooring buoy is connected to the wind turbine floaters. A bearing is attached to the upper connection part, so that the wind turbine floating body can rotate around the mooring buoy floater. There are four mooring points at the bottom part of the buoy, and each point is tensioned by a mooring anchor. Mooring buoy is ballasted with a weight of 8 kg to arrive at required stability. Table 2 summarizes the mooring buoy characteristics.

**Table 2** Principal particulars of mooring buoy floater (equipped with a wind turbine)

| Item | Unit | Scale Model | Actual Model |
|---|---|---|---|
| Mass | ton | 0.02 | 811.81 |
| Draft | m | 0.45 | 16.20 |
| KB | m | 0.34 | 12.24 |
| KG | m | 0.26 | 9.36 |
| BM | m | 0.006 | 0.22 |
| GM | m | 0.08 | 3.16 |

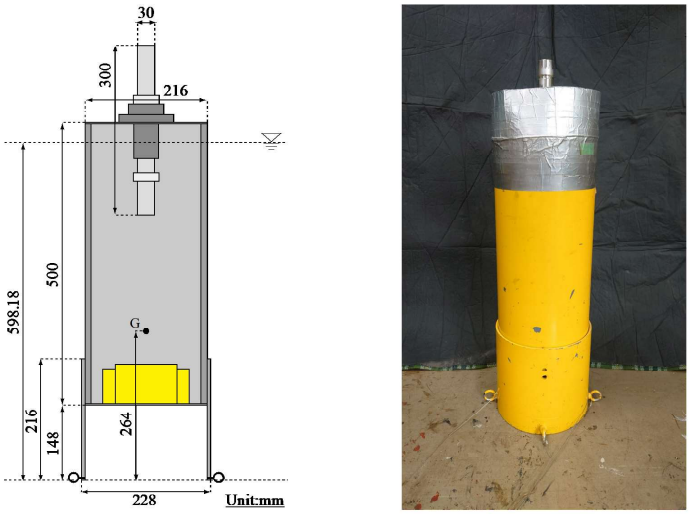


**Fig. 7** Mooring buoy floater

# 4 Physical model

## 4.1 Turning motion simulation

The purpose of this study is to clarify the mechanism of the turning motion of the Multi-connection VAWTs. The design load of the twin turbine system proposed in this study has not been clarified. Therefore, we calculate the design load from experiments and numerical calculations. We construct a program to solve the equations of motion based on the developed mechanical model.

The numerical analysis method for the turning motion used in this study is the Runge-Kutta-Gill method, which is an improved version of the classical Runge-Kutta method. The numerical analysis method is excellent in automatically correcting rounding errors and securing memory space. This numerical method is used to predict the turning motion of the test model. The effect of moored floater is not considered in this numerical simulation. In this study, calm sea areas such as aquaculture farms are assumed. Therefore, the influence on the surge, sway, roll and pitch motions is considered to be negligible. Further, since the mooring attached to the floating structure is a TLP, the heave motion response is small.

### 4.1.1 Equation of motion

Figure 8 shows the coordinate system. The simulations in this study are in a body-fixed coordinate system and the coordinate system also moves with the Yawing of the model, as shown in Figure 8 (b).

Here, G represents the overall center of gravity, and $G_{WT}$ and $G_{WF}$ represent the center of gravity of the wind turbine and the floating structure, respectively. Although a model with six degrees of freedom is shown, in order to simulate the turning motion, the four degrees of freedom equations are solved. The motion responses in heave and pitch are considered to be small and therefore four-degree maneuvering equations of motion is solved for the mechanical model. The equations of maneuvering motion in surge, sway, roll, and yaw can be written as in Eq. 1.

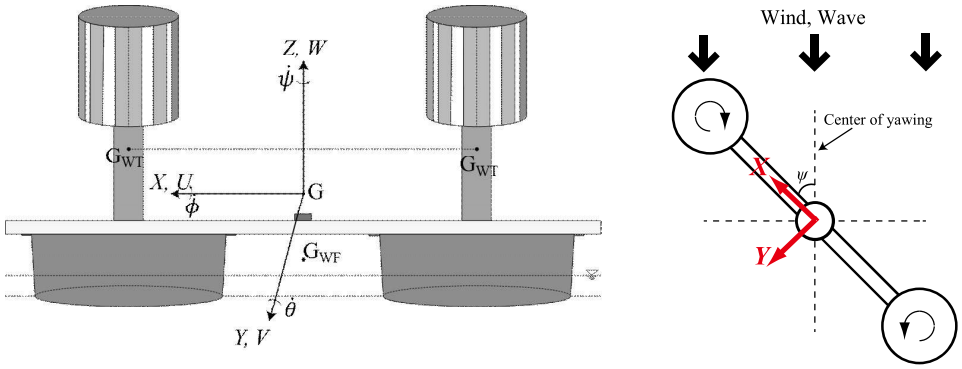


(a) XYZ coordinate (b) X-Y axis

**Fig. 8** The coordinate system of simulation

$$
\begin{aligned}
&(m+m_x)\dot{U} - (m+m_y\cos^2\phi + m_z\sin^2\phi)V\dot{\psi} = F_x \\
&(m+m_y\cos^2\phi + m_z\sin^2\phi)\dot{V} + (m+m_x)U\dot{\psi} \\
&+ 2(m_z - m_y)\sin\phi\cos\phi\cdot V\dot{\phi} = F_y \\
&(I_{xx}+J_{xx})\ddot{\phi} - \{(I_{yy}+J_{yy}) - (I_{zz}+J_{zz})\}\sin\phi\cos\phi\cdot\dot{\psi}^2 = M_x \\
&\{(I_{yy}+J_{yy})\sin^2\phi + (I_{yy}+J_{yy})\cos^2\phi\}\ddot{\psi} \\
&+ 2\{(I_{yy}+J_{yy}) - (I_{zz}+J_{zz})\}\sin\phi\cos\phi\cdot\dot{\psi}\dot{\phi} + b\dot{\psi} = M_z
\end{aligned}
\tag{1}
$$

where $m$ is the mass, $m_x$, $m_y$ and $m_z$ are the added mass, $I_{xx}$, $I_{yy}$ and $I_{zz}$ are the moments of inertia, and $J_{xx}$, $J_{yy}$ and $J_{zz}$ are the added moments of inertia. $U$ and $V$ are linear velocities in surge and sway directions, $\phi$ and $\psi$ are angular displacements in roll and yaw directions. $F_x$ and $F_y$ are loads, and $M_x$ and $M_z$ are moments in surge, sway, roll and yaw directions. In addition, $b$ is the slow-drift damping coefficient.

Here, the roll motion of the mechanical model is small i.e., $\ddot{\phi} = \dot{\phi} = 0$ in the steady-state turning condition. The kinematic model in roll direction can

be assumed as shown in Figure 9. The mooring float hardly tilts and therefore, the moment of roll acting only on the wind turbines is considered. The roll moment can thus be obtained as follows.

$$M_x = -mg\overline{GM}\sin\phi + M_{wind} + M_r + M_{wave} \tag{2}$$

where $M_{wind}$ is the moment due to wind load, $M_r$ is the moment due to hydrodynamic resistance of water, $M_{wave}$ is the moment due to wave load.

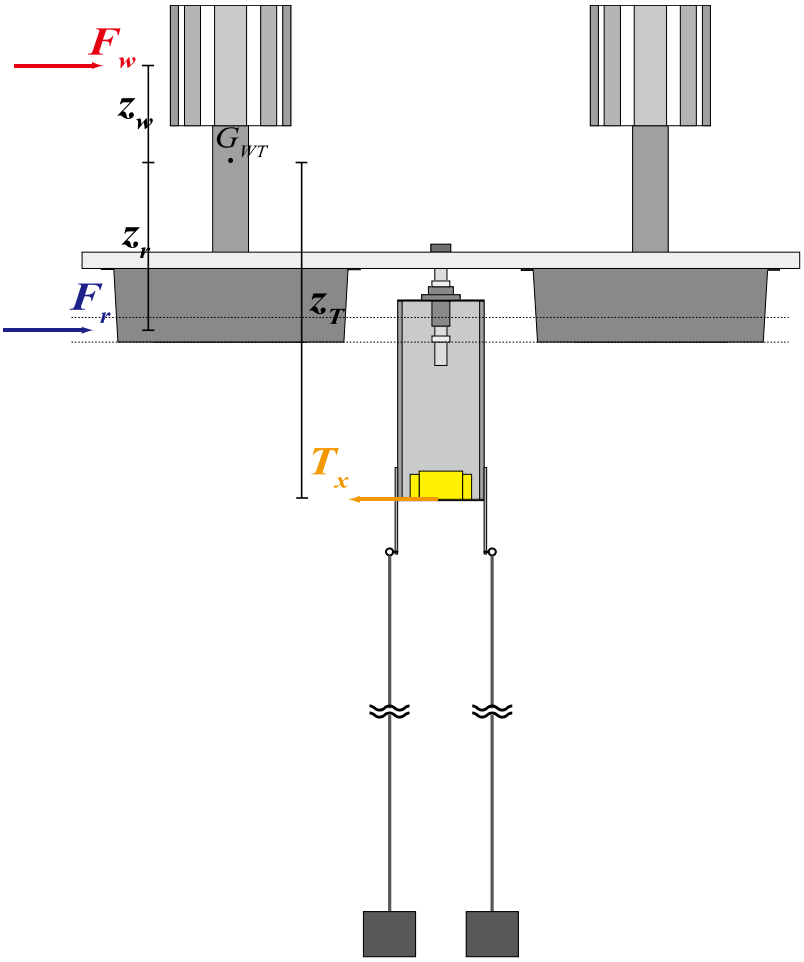


**Fig. 9** Rolling of kinematic model.

Using Equation 2 in the roll equation of motion, the roll angle can be obtained as follows.

$$\begin{aligned} mg\overline{GM}\sin\phi = {} & M_{wind} + M_r + M_{wave} \\ & + \{(I_{yy} + J_{yy}) - (I_{zz} + J_{zz})\}\sin\phi\cos\phi\cdot\dot{\psi}^2 \end{aligned} \tag{3}$$

Where $M_{roll}$ is the right side of Eq. 3, the roll angle is shown in Eq. 4.

$$\phi = \sin^{-1} \frac{M_{roll}}{mg\overline{GM}} \tag{4}$$

Further, Figure 10 shows the kinematic model of the twin-turbines under only-wind condition in yaw direction at an angle of $\psi$

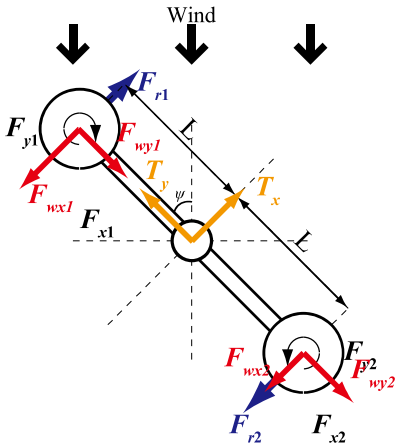


**Fig. 10** Yawing of kinematic model.

The loads acting on this model are the wind load, fluid load resisting the motion, and the mooring load. As the wind blows and the model turns, the external loads acting on the floating body can be modelled as shown in Eq. 5.

$$\begin{aligned} F_x &= F_{wx1} - F_{r1} + F_{wx2} + F_{r2} - T_x \\ F_y &= F_{wy1} + F_{wy2} - T_y \\ M_x &= -(F_{wx1} + F_{wx2})z_w - (F_{r1} - F_{r2})z_r \\ M_z &= (F_{wx1} - F_{wx2})L - (F_{r1} + F_{r2})L \end{aligned} \tag{5}$$

Here, $F_{wx1}$ and $F_{wx2}$ are the wind loads acting on the wind turbines in the longitudinal direction. $F_{wy1}$ and $F_{wy2}$ are wind loads acting on the wind turbines in the transverse direction. $F_{wr1}$ and $F_{wr2}$ are the fluid resistance acting on the wind turbine floats. $T_x$ and $T_y$ are the restoring mooring line forces. $L$ is the distance from the center of turning (the center of the mooring buoy float) to the center of twin wind turbines on either side.

### 4.1.2 Wind load

During the turning motion, the wind speed and correspondingly the wind load acting on the turbine changes depending on the rotational speed of the test model. It is therefore necessary to evaluate relative wind speed acting on each

of the twin turbines. The relative wind speed of test model is obtained by the wind it receives during the turning motion as shown in Figure 11.

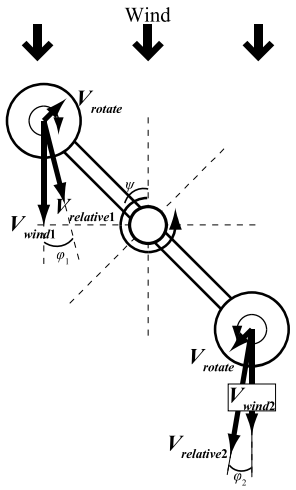


**Fig. 11** Relative wind speed.

where $V_{wind}$ is the wind speed generated at the wind tunnel, $V_{rotate}$ is the speed of the test model as it turns, $V_{relative}$ is the relative wind speed, $\psi$ is the yaw angle of turn, and $\varphi$ is the relative wind speed direction.

$$\begin{aligned} V_{rotate} &= \psi \times L \\ V_{relative1} &= \sqrt{(V_{rotate}\cos\psi)^2 + (V_{wind1} - V_{rotate}\sin\psi)^2} \\ V_{relative2} &= \sqrt{(V_{rotate}\cos\psi)^2 + (V_{wind2} + V_{rotate}\sin\psi)^2} \\ \varphi_1 &= \tan^{-1}\frac{V_{rotate}\cos\psi}{V_{wind1} - V_{rotate}\sin\psi} \\ \varphi_2 &= \tan^{-1}\frac{V_{rotate}\cos\psi}{V_{wind2} + V_{rotate}\sin\psi} \end{aligned} \tag{6}$$

Figure 12 shows the wind loads based on the relative wind velocity as discussed above.

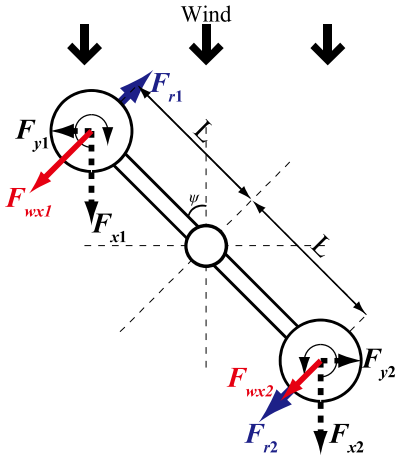


**Fig. 12** A dynamic model considering relative wind speed.

The following equation shows the wind load in the direction of the turning movement when using the relative wind speed obtained from Figure 12.

$$F_{wx1} = \frac{1}{2} C_{dv} \rho_a V_{relative1}^2 S_v \sin(\psi - \varphi_1) + F_{y1} \cos(\psi - \varphi_1)$$
$$F_{wx2} = \frac{1}{2} C_{dv} \rho_a V_{relative2}^2 S_v \sin(\psi + \varphi_2) + F_{y2} \cos(\psi + \varphi_2) \quad (7)$$

where $F_{wx1}$ is the combined force of the wind load on the vertical-axis wind turbine in the clockwise direction in the direction of gyration, $F_{wx2}$ is the combined force of the wind load on the vertical-axis wind turbine in the semi-clockwise direction in the direction of gyration, $C_{dv}$ is the coefficient of efficacy of the vertical-axis wind turbine obtained from the wind load test, $\rho_a$ is the density of air, $S_v$ is the projected area of the vertical-axis wind turbine, and $F_{y1}$ and $F_{y2}$ are the wind load in the direction perpendicular to the wind direction of the vertical-axis wind turbine obtained from the wind load test, $V_{relative}$ is the relative wind speed, $L$ is the distance from the center of gyration to the position of force, $\psi$ is the angle of gyration, and $\varphi$ is the wind direction of the relative wind speed.

In addition, a wind load test was conducted separately on each of the twin vertical axis wind turbines. Figure 13 shows the experimental setup and the schematic diagram of the wind load test. The wind turbine model was fixed to a pedestal with a force gauge. The wind speed was measured simultaneously with a hot wire anemometer placed next to the wind turbine.

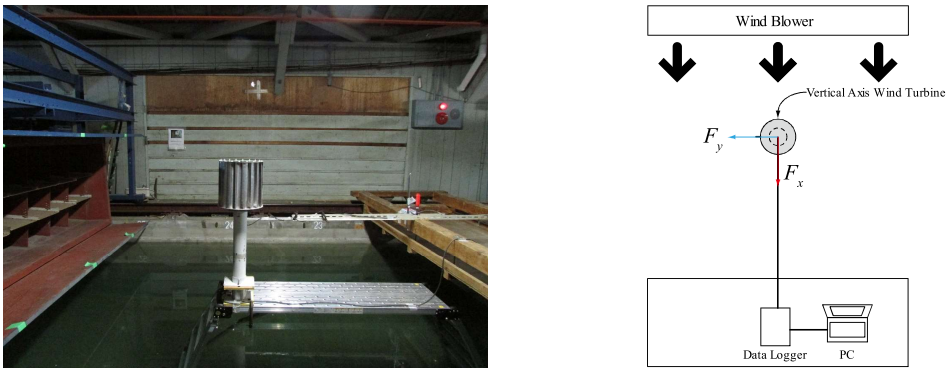


(a) Installed model (b) Schematic view

**Fig. 13** Overview of wind load test

Figure 14 shows the wind loads and drag coefficients acting on the vertical axis wind turbines measured from the wind load test. $C_L$ in the diagram is a coefficient of $F_y$ obtained from wind load tests and is referred to as the lift coefficient for convenience. Where $C_{dv}$ and $C_L$ are shown in Eq. 8. From the test results, the horizontal loads are almost the same for the two wind turbines, while the vertical forces are slightly different. The drag coefficient $C_{dv}$ in the simulation is set to 1.6, which is the average of all the values.

$$C_{dv} = \frac{F_x}{\frac{1}{2}\rho_a V_{wind}^2 S_v}$$
$$C_L = \frac{F_y}{\frac{1}{2}\rho_a V_{wind}^2 S_v} \tag{8}$$

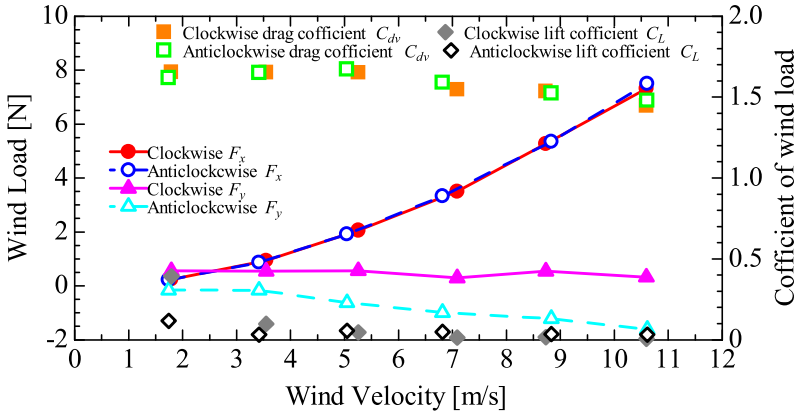


**Fig. 14** Wind load and drag coefficient of wind turbine

### 4.1.3 Mooring line response

In the water tank tests, the mooring buoy was tension moored using four wires. However, in the simulation, the tension load is modelled as a single mooring

cable since the distance between the four tension moorings is short. In this section, the derivation of the constant $k$ for the tension mooring is described. Figure 15 shows the dynamic mooring model before and after moving the buoy.

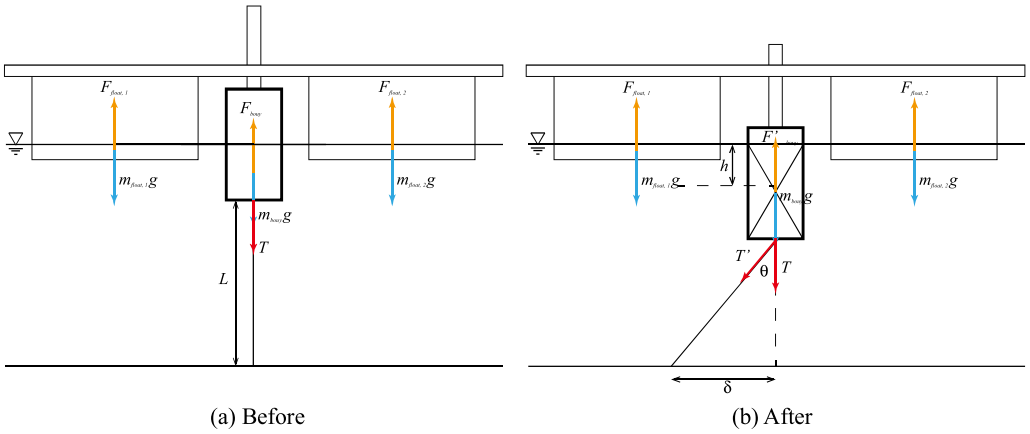


(a) Before (b) After

**Fig. 15** Modelling of mooring force.

$$(F_{buoy} + F_{float,1} + F_{float,2}) - (m_{buoy} + m_{float,1} + m_{float,2})g - T = 0 \quad (9)$$

Suppose the mooring float moves by $\delta$ and the mooring cable tilts by $\theta$. Assuming that the length of the mooring cable $L_{moor}$ is constant, the mooring buoy float will sink by $(1 - \cos\theta)L_{moor}$, and the resulting buoyancy force $F'_{buoy}$ after the change can be expressed by the following equation. In this test model, the joint between the mooring float and the wind turbine floats has a mechanism that allows to freely move up and down. Therefore, even if the whole model moves by $\delta$, the windmill float will not sink by $(1 - \cos\theta)L_{moor}$.

$$F'_{buoy} = F_{buoy} + A_{buoy}h\rho g \quad (10)$$

Here, the depth $h$ due to movement is expressed by the following equation.

$$h = L - \sqrt{L^2 - \delta^2} \quad (11)$$

The tension of the mooring cable in the vertical and horizontal directions is as follows

$$\begin{aligned} T_x &= T' \sin\theta \\ T_y &= T' \cos\theta \end{aligned} \quad (12)$$

The vertical and horizontal equilibrium equations after displacing the mooring float can be expressed as follows.

$$(F'_{buoy} + F_{float,1} + F_{float,2}) - (m_{buoy} + m_{float,1} + m_{float,2})g - T' \cos\theta = 0$$

(13)

$$T' \sin\theta - k\delta = 0 \tag{14}$$

From the equilibrium equations, the spring constant $k$ and movement of the mooring cable can be obtained.

$$k = \frac{F'_{buoy} + F_{float,1} + F_{float,2} - (m_{buoy} + m_{float,1} + m_{float,2})g}{L\cos\theta} \tag{15}$$

$$\theta = \sin^{-1}\frac{\delta}{L} \tag{16}$$

Using the spring constant $k$ obtained above, the mooring cable tensions, $T_x$ and $T_y$ acting on mooring float in the $x$ and $y$-directions can be determined. The purpose of such modelling is to include the effect of changing buoyancy as the mooring float sinks.

## 4.2 Added moment of inertia and Damping force coefficient

Additional moment of inertia and slow-drift damping coefficient are necessary to solve the turning motion of a floating body, and Nihei et al (2020) stated that the damping force is important for the turning motion of a floating wind turbine moored at a single point. Therefore, in this study, a forced yawing test was conducted and these values were obtained from the experiment.

In this test, only the floating part of the 1/72 scale model wind turbine was used to measure the load due to water acting on the floating part. The experimental setup is shown in Figure 16 (a), and the definition of the coordinate system and the load to be measured is shown in Figure 16 (b). The yawing device shown in Figure 16 is connected to a dedicated controller, that sends angle and time data to the yawing device. The yawing device then rotates the attached model and the load in each direction was measured with a force gauge. These measured forces are post-processed to obtain added moment of inertia and damping force coefficient.

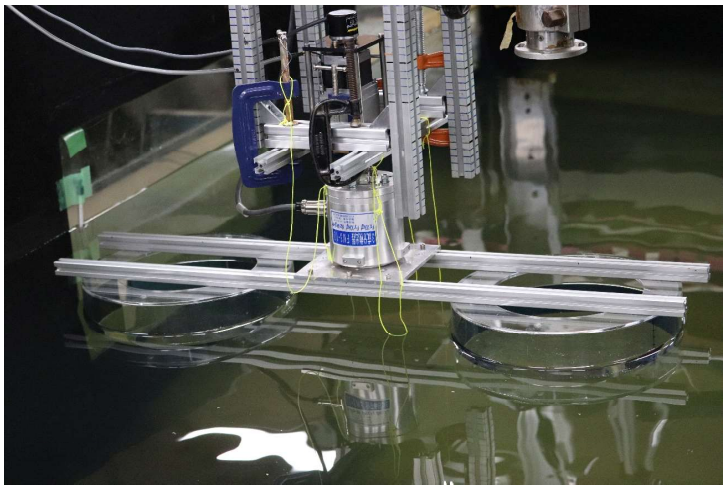

(a) Installed model

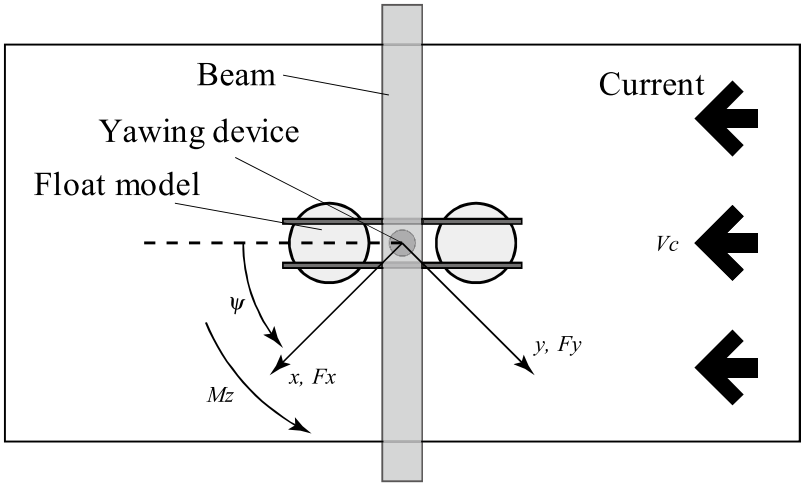


(b) Coordinate system

**Fig. 16** Forced yawing test (1/72 scale model).

**Table 3** Forced yawing test conditions

| Item | Unit | Value |
|---|---|---|
| Period $T$ | s | 5, 10, 15∼40, 50 |
| Amplitude $A$ | deg | 5, 10, 20∼60 |
| Center of yawing $B$ | deg | 0, 90 |
| Current speed $V_c$ | cm/s | 0, 0.2 |

## 4.3 Wave load

The wave loads acting on the two floating wind turbines are obtained by using a hybrid boundary element method based on potential theory, which was developed by Masuda et al (1993). The fluid domain is divided into two regions,

inner and outer. The outer region is solved by the eigenfunction expansion method, while the inner region is solved by the boundary element method using a simple ranking source of Green's functions. This makes it possible to mathematically handle even non-dominant forces of arbitrary shape in higher-order hydrodynamic calculations.

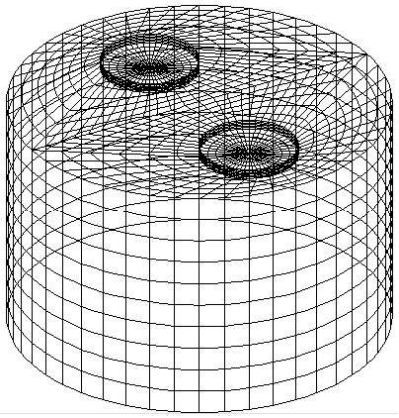

**Fig. 17** HYBIEM mesh modele

The roll angle can be calculated using equation 17 when only waves are acting and the floating body is not in yawing motion. Here, the moment acting on the floating body is $M$. The same equation can be used to determine the roll and pitch angles when only wind acts on the floating body.

$$\phi = \sin^{-1} \frac{M}{mg\overline{GM}} \tag{17}$$

## 4.4 Numerical simulation

Table 4 summarizes the simulation conditions.

**Table 4** Simulation conditions

| Item | Unit | 1/36 Scale model |
|---|---|---|
| Rotational inertia of float $I_{zz}$ | kg | 8.73 |
| Added mass of float and buoy $m_x, m_y$ | kg | 25.09 |
| Added rotational inertia of float and buoy $J_{xx}, J_{yy}$ | kgm$^2$ | 16.55 |
| Added rotational inertia of float $J_{zz}$ | kgm$^2$ | 6.45 |
| Density of water $\rho_w$ | kg/m$^3$ | 1000 |
| Density of air $\rho_a$ | kg/m$^3$ | 1.293 |
| Drag coefficient of float $C_{Dwf}$ | - | 0.9 |
| Drag coefficient of wind turbine $C_{Dwt}$ | - | 1.60 |
| Damping force coefficient $b$ | kgm$^2$ | 0.526 |
| Mooring length $L$ | m | 1.0 |

# 5 Water tank test in wind and wave

The turning motion experimental setup is shown in Figure 18 (a) and conducted for various initial positions of the model as defined in Figure 18 (b). For the motion measurements, multiple trackers are mounted on to the test model and OptiTrack's motion capture cameras are utilized. The test model is regarded as a rigid body, and in this tank test, eight trackers were mounted on a steel frame.

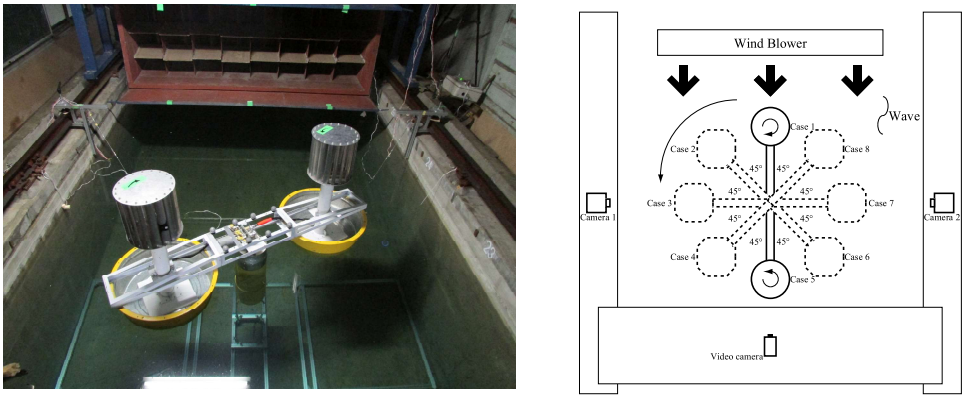


(a) Installed model (b) Definition of initial positions

**Fig. 18** Experimental setup.

The experimental conditions are shown in Table 5. The wind speed is set to 7 m/s at which the vertical axis wind turbine could rotate moderately. The wave heights and wavelengths are based on the wave conditions assuming that the test model is 1/36 scale.

**Table 5** Experimental conditions of turning motion test

| Item | Unit | 1/36 Scale Model | Actual Model |
|---|---|---|---|
| Initial positions | deg | 0, 45 ∼ 315 | 0, 45 ∼ 315 |
| Wind speed | m/s | 7.0 | 42.0 |
| Wave height | m | 0.03 | 1.08 |
| Wave period | s | 1.0 ∼ 1.5 | 6.0 ∼ 9.0 |

# 6 Results and discussion

## 6.1 Effects of wind

Figure 19 shows the turning motion obtained from the wind-only test results for Case2, Case 3, Case 5 and Case 7. Here, the initial positions for Case 2, Case 3, Case 5 and Case 7 are 45, 90, 180 and 270 deg. In the wind-only tests, the turning motion converged at 90 deg for all the different initial positions. In Case 3, it can be seen that the model did not move from the initial position

since both the wind turbines faced the wind. Therefore, it was expected that in Case 7 does not move from the initial position since both wind turbines face the wind. However, Case 7 turned and converged to a final position of 90 deg. The only difference between Case 3 and Case 7 is that the initial positions of the two wind turbines is interchanged. Since the horizontal wind load acting on both clockwise- and counterclockwise- rotating turbines are same, it is hypothesized that the small vertical wind load (as in Fig 14) contributes to such turning motion.

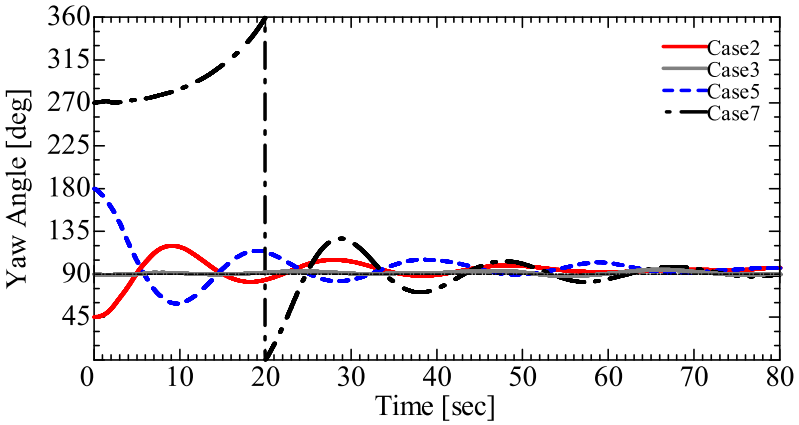


**Fig. 19** Experimental results in wind-only condition.

Figure 20 and Figure 21 show the comparison between the simulation and the wind-only test for Case 1 and Case 8, respectively. In the simulation, the small vertical wind load obtained from the wind load test is also considered and we can observe good correlation between calculation and experimental result. Such results could not be obtained if only the horizontal wind load was considered in the calculations. This suggests that loads acting on each wind turbine needs to be accurately modelled when hosting multiple turbines.

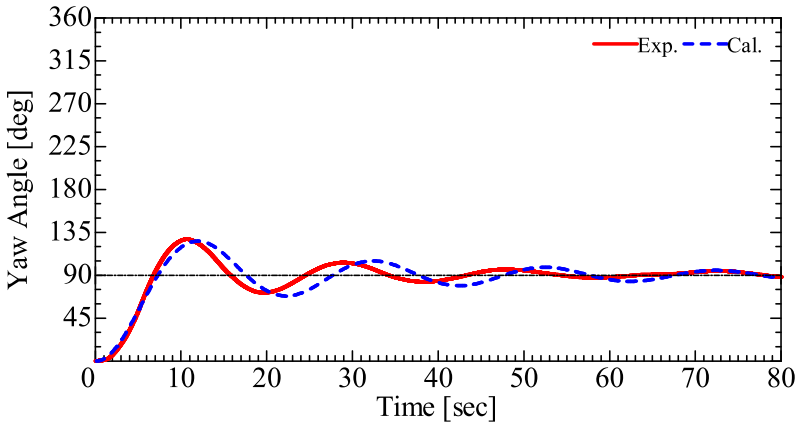


**Fig. 20** Comparison between experiment (only wind) and simulation - Case 1.

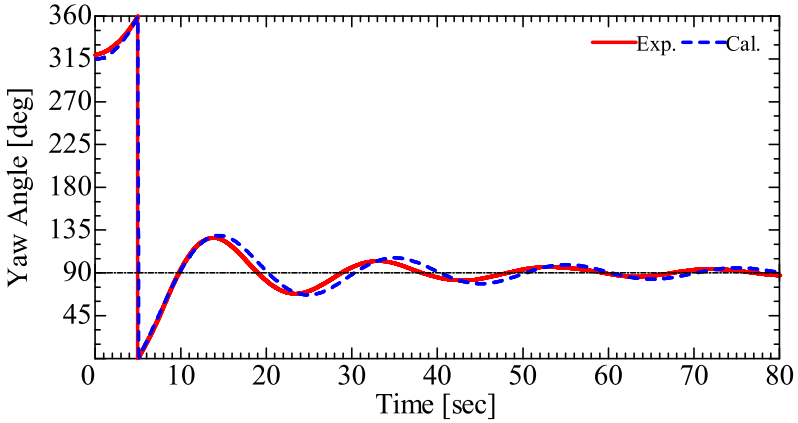


**Fig. 21** Comparison between experiment (only wind) and simulation - Case 8.

Now to understand the wind load distribution during the simulation, Figure 22 shows the variation between clockwise and anticlockwise rotating turbines for Case 1. The wind load difference between the left (clockwise rotating) and right (anticlockwise rotating) turbines becomes smaller as we approach the final position of 90 deg. From this result, it can be said that the load generated inside the wind turbine is important for the turning motion prediction. In other words, it can be said that the motion of a multi-turbine floating wind turbine, converges at the point where the external forces acting on the left and right sides are balanced when two vertical axis wind turbines are symmetrically mounted.

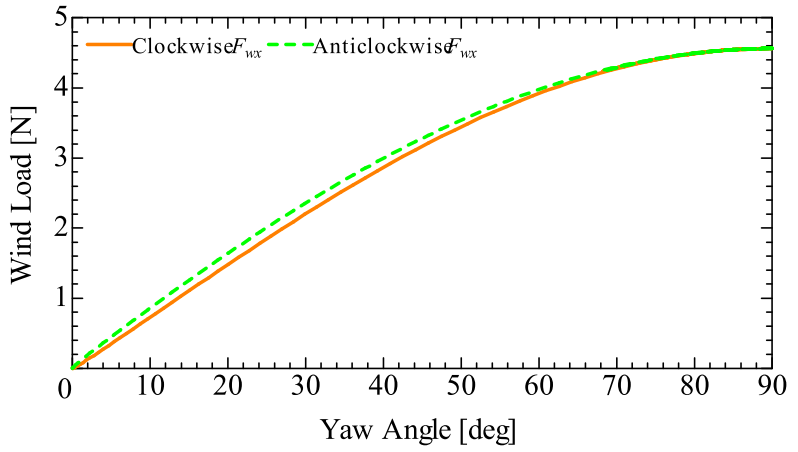


**Fig. 22** Wind load distribution during turning motion - Case 1.

## 6.2 Effects of wave

Figure 23 shows the comparison between the wave-only test and the simulation for Case 2 with a wave height of 0.03 m and a wave period of 1.0s (real wave period of 6.0 s). Both the experimental and calculation results of the wave-only condition show that the model did not move much and is unaffected by the waves.

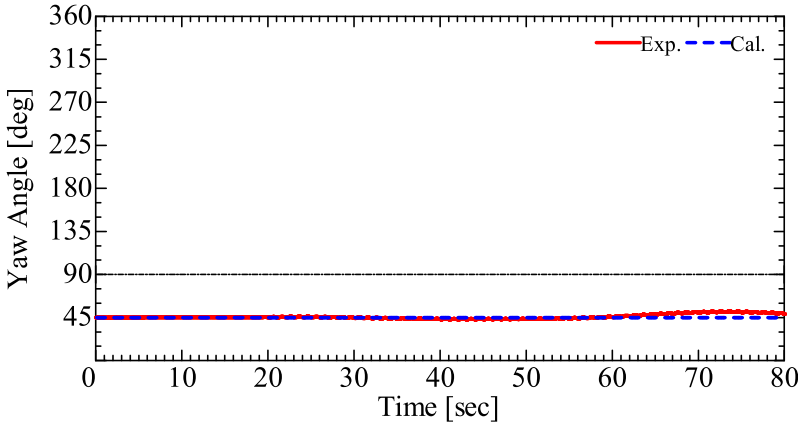


**Fig. 23** Comparison between experiment (only wave) and simulation - Case 2

Figure 24 shows the roll angle for the 1/36 scale model with a wave height of 0.03 m, a wave period of 1.5 s and wind velocity 7.0 m/s. This result was calculated from Eq. 17. As can be seen from the graph, the roll angle is less than 1.5 deg, which is quite small. From this result, it can be said that the effect of waves on the model is small. In this study, the wave loads obtained in this frequency domain are put into the time domain.

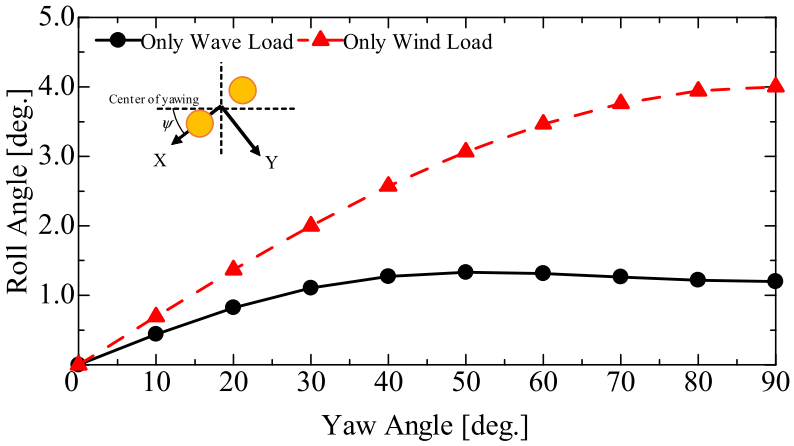


**Fig. 24** Roll angle for the 1/36 scale model.

## 6.3 Effects of wind and wave

Figure 25 shows the experimental results of wind-only and wind-wave coexisting conditions for Case 1. The results for wave height of 3.0 cm and wave period of 1.0 and 1.5 s (real wave period of 6.0 and 9.0 s) is shown. It can be observed that the maximum yaw angle was 127 deg in wind-only condition and time required to turn was about 10 seconds. In contrast, under the wind-wave coexisting condition, the maximum yaw angle decreased to 120 and 121 degrees, for wave periods of 1.0 and 1.5 seconds, respectively. However, the time taken to turn increased to 12 and 11 seconds. From these results, it can be seen that there is almost no difference between the wave periods of 1.0 and

1.5 seconds for initial position of 0 deg. A similar trend was observed in the other cases, and little difference was observed between the waves.

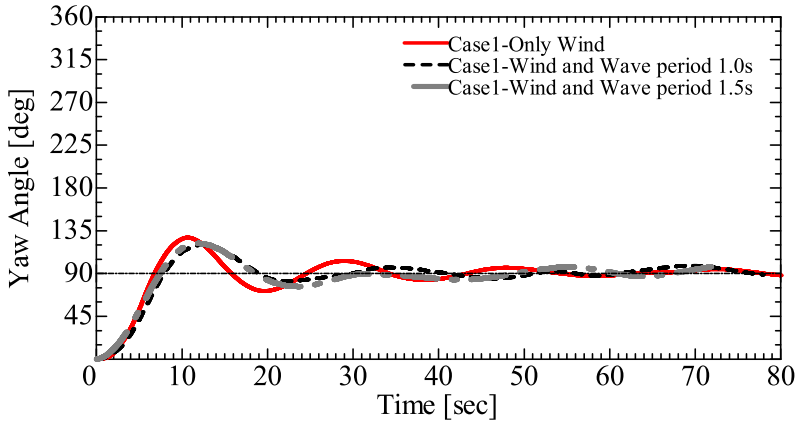


**Fig. 25** Experimental result of wind-only and wind-wave conditions - Case 1

Figure 26 shows the comparison between the wind-wave coexisting test and the simulation for Case 5 with a wave period of 1.1 s (real wave period 6.6 s) and a wave height of 3.0 cm. As mentioned earlier, the effect of the waves is limited and the experimental and simulation results generally agreed in this simulation. However, there is a slight difference between experiment and simulation results around the elapsed time of 20 s, where the maximum yaw angle was 106 deg at 23.8 s in the experiment and 111 deg at 22 s in the simulation. This slight error, 5%, is thought to be due to the moment of inertia of the small parts installed in the model, which is not considered in the simulation. In other cases, the difference between the experimental and calculated values shows an error of less than 10%. However, it can be said that the accuracy of the simulation is sufficient to understand the basic principal involved in hosting multiple vertical axis wind turbines.

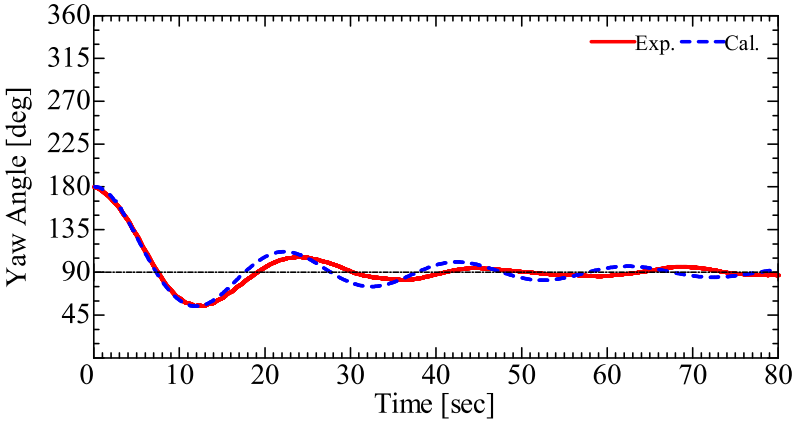


**Fig. 26** Comparison between experiment (wind-wave) and simulation - Case 5

# 7 Conclusion

In this study, a new-type floating offshore wind turbine is proposed, which consists of two wind turbine floats hosting cross-flow type wind turbines connected to a mooring float in a straight line. The motion response and wind-following performance of the prototype model is experimentally clarified from free yawing tests in wind and wave conditions using a 1/36 scale model. In addition, a time history program was developed using a four-degree-of-freedom maneuvering equation to simulate the turning motion of the floating structure. The findings of this study are summarized as follows.

- The floating wind turbines turned around the mooring float and converged to a final position facing the wind, irrespective of different initial positions. From the experiments, it was found that the two cross-flow wind turbines rotated after receiving adequate wind at the converged position. It is therefore expected to generate power using the proposed concept.
- From the simulation and the experimental results, it is found that the turning motion of the floating wind turbine converges to a final position where the loads acting on the left and right wind turbines are balanced. It is therefore important to accurately evaluate not only in-line wind load but also transverse wind load acting on the turbines.
- It is found that the floating model in this study is almost unaffected by waves under long wave period conditions. It can be concluded that the prototype model is suitable to be installed at aquaculture farms where the wave conditions are relatively calm.
- In this study, a numerical model of a multi-connected floating wind turbine is developed and compared with experimental results. The error between the simulation and the experimental results is within 10% throughout the entire model, which is sufficiently accurate. This error can be reduced by accurately considering the moment of inertia of small parts in the model.

# Conflict of interest

The authors declare no conflicts of interest associated with this manuscript.

# References

Alkan S (2017) Comparative hydrodynamic analysis of catenary and tension leg moored floating offshore wind turbine. 1st International Conference on Energy Systems Engineering, Karabuk, Turkey, 2–4 Nov 2017

Frank RE (1980) Wind Machines 2nd Edition, The MITRE Energy Resources and Environment Series. Van Nostrand Reinhold Company, New York

Giorgetti S, Pellegrini G, Zanforlin S (2015) Cfd investigation on the aerodynamic interferences between medium-solidity darrieus vertical axis wind turbines. Energy Procedia 14:227–239

Iijima K, Kuroda Y, Nihei Y, et al (2015) Comparison of weathervane performance between two types of fowt systems moored to spm. ASME 2015 34th International Conference on Ocean, Newfoundland, Canada, 31 May –5 Jun 2015

Iwamatsu S, Nihei Y, Iijima K, et al (2021) Experimental study on the stability performance and turning motion of multi - connection vawt. ASME 2021 40th International Conference on Ocean, Virtual, Online, 21–30 Jun 2021

Kikuchi Y, Namba H, Ishihara T (2017) A study of dynamic responses of several floating foundation concepts. 39th Symposium on Wind Energy Utilization, Tokyo, Japan, 6–7 Dec 2018, https://doi.org/10.11333/jweasympo.39.0_315

Kusanagi K, Srinivasamurthy S, Nihei Y (2018) Slewing effect of twin vertical axis wind turbines supported by a floating platform able to rotate around a single mooring system. ASME 2018 37th International Conference on Ocean, Madrid, Spain, 17–22 Jun 2018

Maeda H, Hodokawa K, Okunishi S, et al (2009) Suppression of red tide by chemicals. Bulletin of the Plankton Society of Japan 56(1):69–73

Masuda K, Nagai T, Gotoh S (1993) Second-order wave exciting forces on column-footing type floating bodies. Proceedings of the Japan Shipbuilding Association 174

Nakata H (2014) Study of performance of a cross-flow wind turbine located above a roadway fence. Kanazawa university

Nihei Y, Srinivasamurthy S, Hashimoto K, et al (2020) Influence of slow-drift damping on the weathervaning of single-point moored floating offshore wind turbines. Ocean Engineering 217(107899)

Philip IDavid (2012) Investigation of the madaras wind turbine using computational tools. Graduate School of Vanderbilt University

Srinivasamurthy S, Iwamatsu S, Hashimoto K, et al (2021) Study of slow-drift damping on wind tracking performance of a new-type fowt ‘optiflow’ with single-point mooring. Ocean Engineering 242(1110131)

Thi TEV, Ko H, Huh J, et al (2021) Overview of solar energy for aquaculture: The potential and future trends. Energies 14(21):6923

Ueno T, Nagaya S, Shimizu M, et al (2018) Development and demonstration test for floating type ocean current turbine system conducted in kuroshio current. OCEANS’18 MTS / IEEE Kobe / Techno-Ocean2018, Hyogo, Japan, 28–31 May 2018, http://dx.doi.org/10.1109/OCEANSKOBE.2018.

8558792

Verdant Power LLC. (2019) Roosevelt island tidal energy project ferc no. p-12611 article 401 rmee plan amendments. Figshare https://tethys.pnnl.gov/publications/roosevelt-island-tidal-energy-project-ferc-no-p-12611-article-401-rmee-plan-amendments

Yamaguchi H, Imakita A (2018) Learning from field test regarding damping of a floater motion - 2MW FOWT "Fukushima Mirai"-. Grand Renewable Energy 2018, Yokohama, Japan, 17–22 Dec 2018